Report

Current Biology

Static Dental Disparity and Morphological Turnover in Sharks across the End-Cretaceous Mass Extinction

Graphical Abstract

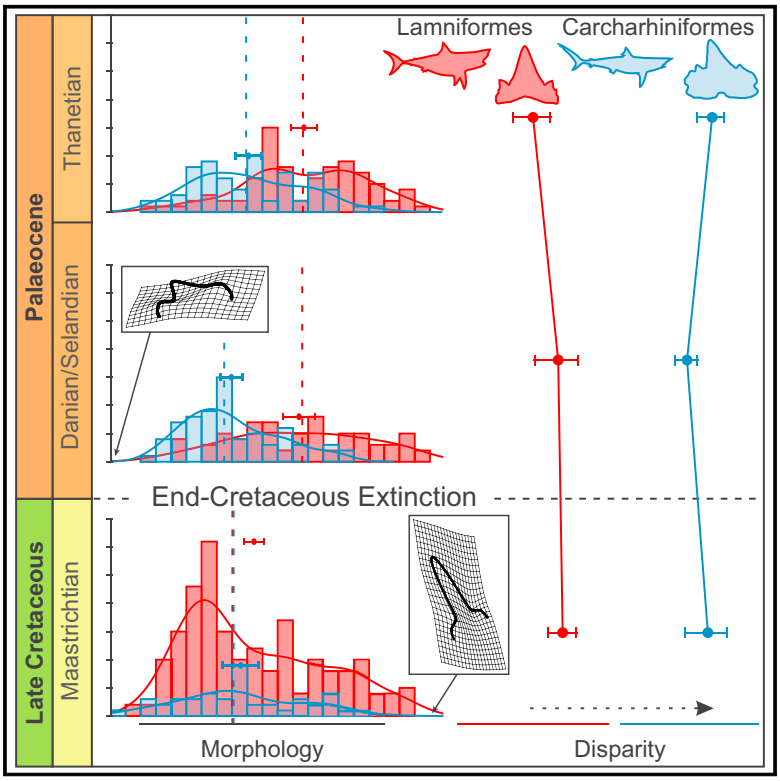

Authors

Mohamad Bazzi, Benjamin P. Kear, Henning Blom, Per E. Ahlberg, Nicolás E. Campione

Correspondence

mohamad.bazzi@ebc.uu.se (M.B.), ncampion@une.edu.au (N.E.C.)

In Brief

Bazzi et al. analyze shark tooth morphology to reconstruct global faunal turnover across the end-Cretaceous mass extinction. Stable disparity, selective extinctions and trophic restructuring collectively favored modern lineage radiations. The composition of living shark communities is thus underpinned by extinction recovery 66 million years ago.

Highlights

- Shark teeth reveal morphological turnover during the end-Cretaceous mass extinction
- Fossil shark dental disparity is decoupled from taxonomic richness
- Cretaceous–Palaeogene shark disparity was nearly static unlike other marine predators
- Prey availability and trophic cascades may have initiated Cenozoic shark radiations

Bazzi et al., 2018, Current Biology *28*, 2607–2615
August 20, 2018
https://doi.org/10.1016/j.cub.2018.05.093

CellPress

Current Biology
Report

Static Dental Disparity and Morphological Turnover in Sharks across the End-Cretaceous Mass Extinction

Mohamad Bazzi,[1,2,5,*] Benjamin P. Kear,[3] Henning Blom,[1] Per E. Ahlberg,[1] and Nicolás E. Campione[1,2,4,*]
[1]Subdepartment of Evolution and Development, Department of Organismal Biology, Uppsala University, Norbyvägen 18A, SE-752 36 Uppsala, Sweden
[2]Palaeobiology Programme, Department of Earth Science, Uppsala University, Villavägen 16, SE-752 36 Uppsala, Sweden
[3]Museum of Evolution, Uppsala University, Norbyvägen 16, SE-752 36 Uppsala, Sweden
[4]Palaeoscience Research Centre, School of Environmental and Rural Science, University of New England, Armidale 2351, New South Wales, Australia
[5]Lead Contact
*Correspondence: mohamad.bazzi@ebc.uu.se (M.B.), ncampion@une.edu.au (N.E.C.)
https://doi.org/10.1016/j.cub.2018.05.093

SUMMARY

The Cretaceous–Palaeogene (K–Pg) mass extinction profoundly altered vertebrate ecosystems and prompted the radiation of many extant clades [1, 2]. Sharks (Selachimorpha) were one of the few larger-bodied marine predators that survived the K–Pg event and are represented by an almost-continuous dental fossil record. However, the precise dynamics of their transition through this interval remain uncertain [3]. Here, we apply 2D geometric morphometrics to reconstruct global and regional dental morphospace variation among Lamniformes (Mackerel sharks) and Carcharhiniformes (Ground sharks). These clades are prevalent predators in today's oceans, and were geographically widespread during the late Cretaceous–early Palaeogene. Our results reveal a decoupling of morphological disparity and taxonomic richness. Indeed, shark disparity was nearly static across the K–Pg extinction, in contrast to abrupt declines among other higher-trophic-level marine predators [4, 5]. Nevertheless, specific patterns indicate that an asymmetric extinction occurred among lamniforms possessing low-crowned/triangular teeth and that a subsequent proliferation of carcharhiniforms with similar tooth morphologies took place during the early Paleocene. This compositional shift in post-Mesozoic shark lineages hints at a profound and persistent K–Pg signature evident in the heterogeneity of modern shark communities. Moreover, such wholesale lineage turnover coincided with the loss of many cephalopod [6] and pelagic amniote [5] groups, as well as the explosive radiation of middle trophic-level teleost fishes [1]. We hypothesize that a combination of prey availability and post-extinction trophic cascades favored extant shark antecedents and laid the foundation for their extensive diversification later in the Cenozoic [7–10].

RESULTS

We reconstructed the morphological succession of shark teeth across the K–Pg boundary using a global dataset of 597 individual tooth crowns representing the spectrum of lamniform and carcharhiniform dental disparity (Figure 1A). Our objectives were to establish the following: (1) whether disparity decreased during the K–Pg extinction, as has been previously interpreted from taxonomic richness [3, 11, 12]; and (2) if certain morphologies (and interpreted ecologies) were selectively targeted, as has been proposed for actinopterygian fishes [4] and reptilian marine amniotes [5]. Furthermore, we utilize a novel approach of assessing global and regional patterns in tandem via a specifically selected local subsample from the UNESCO World Heritage K–Pg section at Stevns Klint in Denmark. Our results reveal not only the complexity of shark extinction and recovery across the K–Pg transition, but also the potential role that prey selection and post-extinction processes played in shark lineage survival during one of the most catastrophic biotic perturbations in Earth history.

Global Morphological Patterns

The first two principal components (PCs) account for approximately 80% of the total variation in our global dental dataset (PC1 = 65.03% and PC2 = 14.52%) and represent the main axes for interpretation in our study (Figure 1B and Table S1). PC1 describes a morphological continuum from positively loaded mesiodistally narrow, apicobasally tall teeth to negatively loaded broad and low-crowned teeth. Both lamniforms and carcharhiniforms are positively skewed along PC1 and are significantly different from normal (Shapiro Test: $W_{lamniforms} = 0.962$, $p << 0.001$; $W_{carcharhiniforms} = 0.976$, $p = 0.002$). These groups also occupy equivalent ranges in morphospace, although relatively more lamniforms load positively, while carcharhiniforms

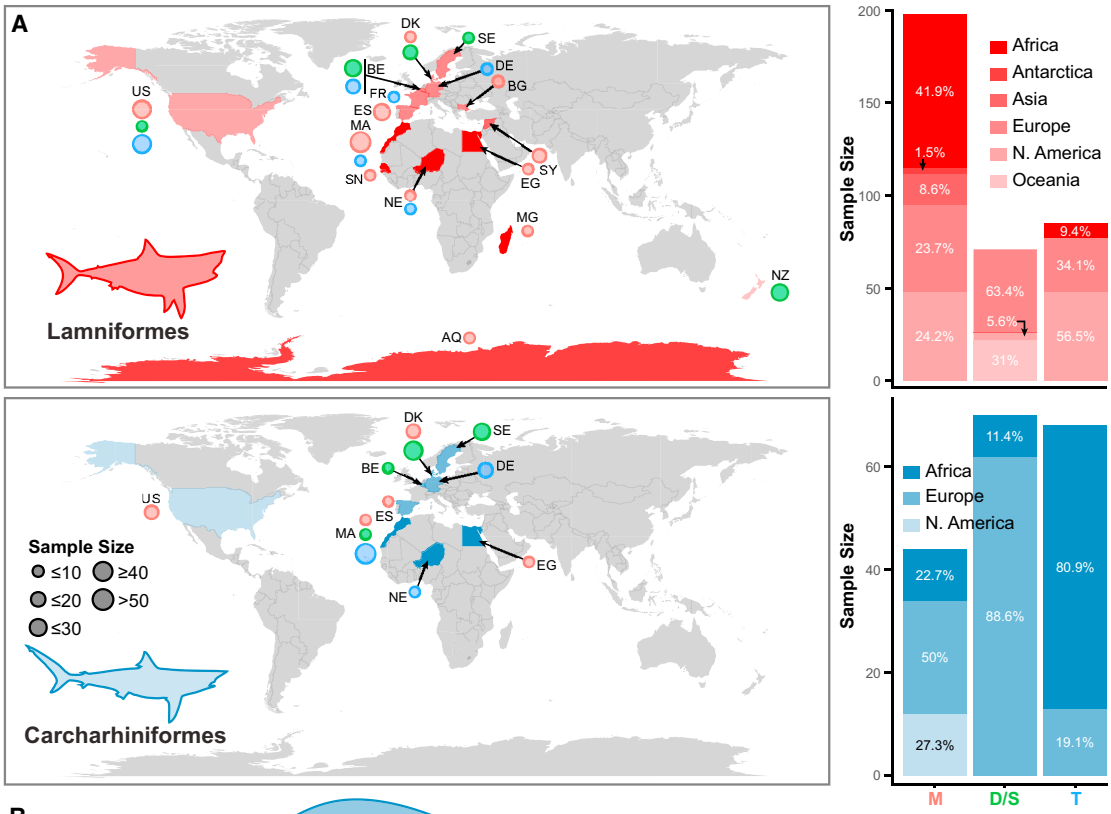

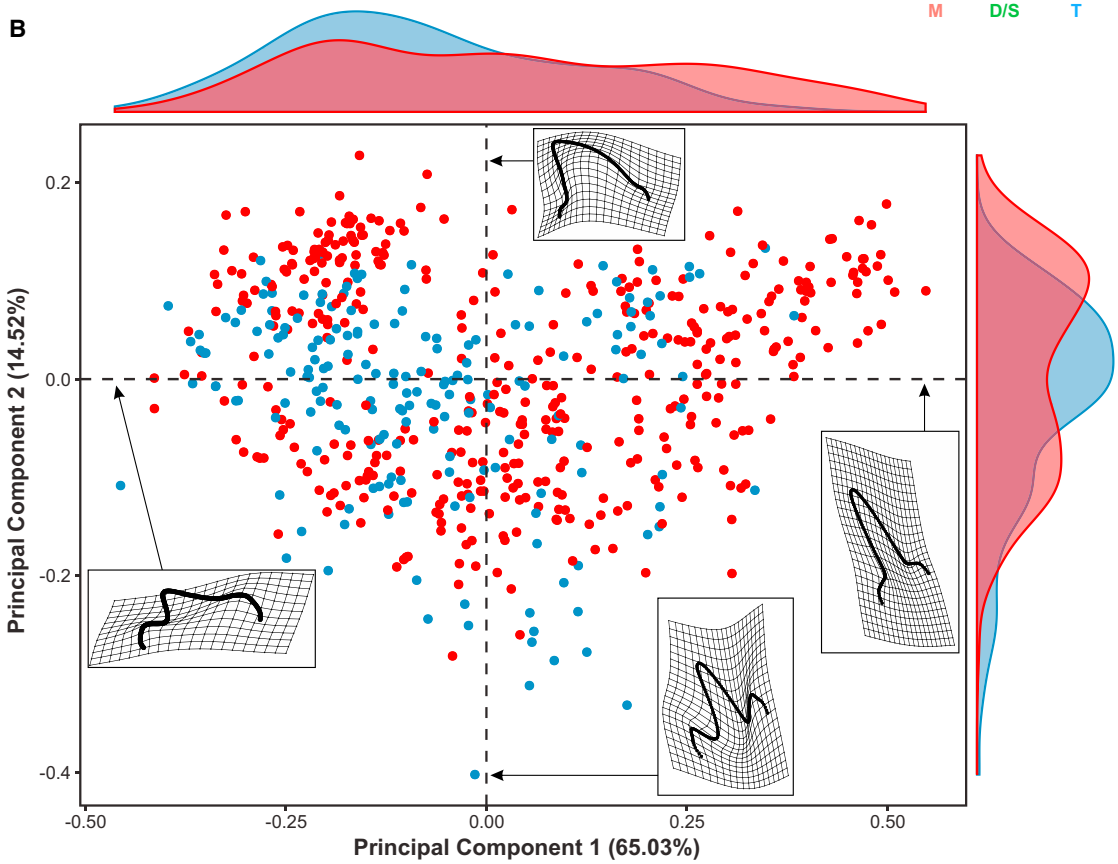

(legend on next page)

tend to negatively load along PC1. PC2 describes the relative development of mesial and distal cusplets along the negative axis, as opposed to increasing mesiodistal width and triangular outline along the positive axis. Lamniforms and carcharhiniforms again occupy equivalent ranges of morphospace, and both are non-normal ($W_{lamniforms}$ = 0.962, p <<0.0001; $W_{carcharhiniforms}$ = 0.923, p <<0.0001). Nevertheless, carcharhiniforms are more negatively skewed with a modal value centered on the average for PC2. Visually, lamniforms appear bimodal along PC2, but we cannot reject unimodality (Hartigan's Dip Test: D = 0.02, p = 0.32). Finally, the morphological gradients described by PC1 and PC2 roughly correspond to recognized functional tooth morphotypes [13], with tall and narrow cusped teeth clustered into tearing and clutching tooth categories (+PC1/–PC2) and low-crowned to increasingly triangular teeth representing the cutting tooth category (–PC1/+PC2).

Morphological Patterns through Time

A general Procrustes ANOVA recovered significant differences in global lamniform morphospace across the K–Pg boundary, but not among carcharhiniforms (Tables S2 and S3). Lamniform sharks are found to have broadly occupied morphospace in the Maastrichtian; however, this distribution contracted substantially by the early Paleocene (Figure 2A). In particular, mesiodistally broad low-crowned teeth, which load negatively along PC1, together with triangular teeth loading positively along our PC2, both seem to have virtually disappeared (Figure 2A). Concomitantly, these areas of morphospace were underutilized by carcharhiniforms during the Maastrichtian but are immediately exploited in the extinction aftermath (Figure 2A and Table S3). Importantly, this pattern does not produce significant alterations in carcharhiniform morphospace along PC1 (P_{ANOVA} = 0.429; P_{KS} = 0.174), although it does result in increased skewness ($g1_{Maastrichtian}$ = 0.189; $g1_{Danain/Selandian}$ = 0.575) and a shift toward non-normality in the early Paleocene (W = 0.957, p = 0.017) versus Maastrichtian (W = 0.975, p = 0.432). There are otherwise no significant changes in morphospace throughout the later Paleocene, nor are there major shifts along the main axes of variation (PC1 and PC2: Table S3). However, lamniforms do exhibit minor adjustments during the Danian and Selandian, as well as in the Selandian and Thanetian when an alternative four-stage time-binning scheme is implemented (Figure S1 and Tables S2 and S4). Carcharhiniforms correspondingly increase their variation in clutching morphotypes, which are negatively loaded along PC2; these equate to morphospace regions that were unexplored prior to the K–Pg boundary (Figure 2A). A significant difference is achieved during the Thanetian along PC2 (Table S3), but this becomes less marked following the imposition of a four-stage binning scheme (p = 0.078: see Figure S1, Table S4).

Our regional subsample of lamniforms from Stevns Klint is small ($N_{lMaastrichtian}$ = 10, $N_{eDanian}$ = 6) and not sufficient for detecting significant changes across the K–Pg boundary (Tables S2 and S5). Nevertheless, the overall pattern of morphospace occupation is comparable to our global-level analysis. For example, late Maastrichtian lamniforms occupy a broad range of morphologies along PC1 (Figure S2), but these contracted during the early Danian and are almost entirely limited to positively loaded morphologies. Carcharhiniforms, on the other hand, are better sampled across the K–Pg interval ($N_{lMaastrichtian}$ = 14, $N_{eDanian}$ = 37) but show no significant shifts in morphospace (Tables S2, S3, and S5). Despite this, there is an increase in negatively loaded morphologies during the early Danian, which results in positive skewness ($g1_{lMaastrichtian}$ = –0.024; $g1_{eDanain}$ = 0.455); this is similar to the result returned by our global sample. Temporal shifts in morphospace along PC2 are much less pronounced, but they reveal a peak among mean carcharhiniform tooth morphologies during the early Danian and a coupled loss of peripheral positively loaded lamniform morphologies across the K–Pg boundary. Notably, our global sample is also geographically biased toward the disproportionately large number of specimens from the Stevns Klint lagerstätte (especially its Danian section), with lamniforms and carcharhiniforms contributing 4.5% and 28% of the total global dataset respectively. To accommodate, we conducted a final validation test that excluded the Stevns Klint subsample, but this had little effect on our overall interpretations relative to the original cross-section of globally distributed fossils (Figure S3).

Disparity Patterns through Time

We find lamniform dental disparity to be nearly static across the K–Pg boundary, with statistically indistinguishable estimates derived for the Maastrichtian and early Paleocene (Figure 2B). The only deviation is among carcharhiniforms, which underwent a slight non-significant decrease in disparity (Figure 2B). Further testing with rarefaction recovered very similar results, indicating that variation in sample size does not affect the overall signal for either clade. Disparity within lamniforms remains stable throughout much of the Paleocene but reduces significantly by the Thanetian compared to its pre-extinction levels ($PV_{Maastriachtian}$ = 0.075; $PV_{Thanetian}$ = 0.059; p = 0.026). Under the four-stage binning scheme, Selandian lamniforms are significantly less disparate than those from either the Danian (PV_{Danian} = 0.068; $PV_{Selandian}$ = 0.033; p = 0.03) or Thanetian ($PV_{Thanetian}$ = 0.059; p = 0.032); a pattern that persists even after subsampling (Figure 2B). In comparison to our global dataset, the Stevns Klint subsample recovered lower levels of regional disparity among lamniforms during the Maastrichtian but was consistent in producing no recognizable shift across the K–Pg boundary (Figure 2B). Alternatively, carcharhiniforms seem to have decreased in disparity between the late Maastrichtian and early Danian ($PV_{l.Maastichtian}$ = 0.08; $PV_{e.Danian}$ = 0.054: Figure 2B), yet our small sample size fails to reject the null hypothesis of no change (p = 0.096).

Figure 1. Global Spatiotemporal and Morphospace Visualizations of Lamniform and Carcharhiniform Sharks

(A) Maps depicting the global distribution of lamniform (red) and carcharhiniform (blue) fossil samples. Stacked bar plots (on right) represent proportions and absolute counts of lamniform and carcharhiniform occurrences by continent and temporal bin.

(B) Bivariate plot of PC1 and PC2 with associated density curves along each axis of variation (see also Table S1). Thin-plate splines represent hypothetical projections of the maximal and minimal loadings of shape coordinates along both axes. Graphic silhouettes reproduced with permission from Gray Taxidermy (Pompano Beach, U.S.A.).

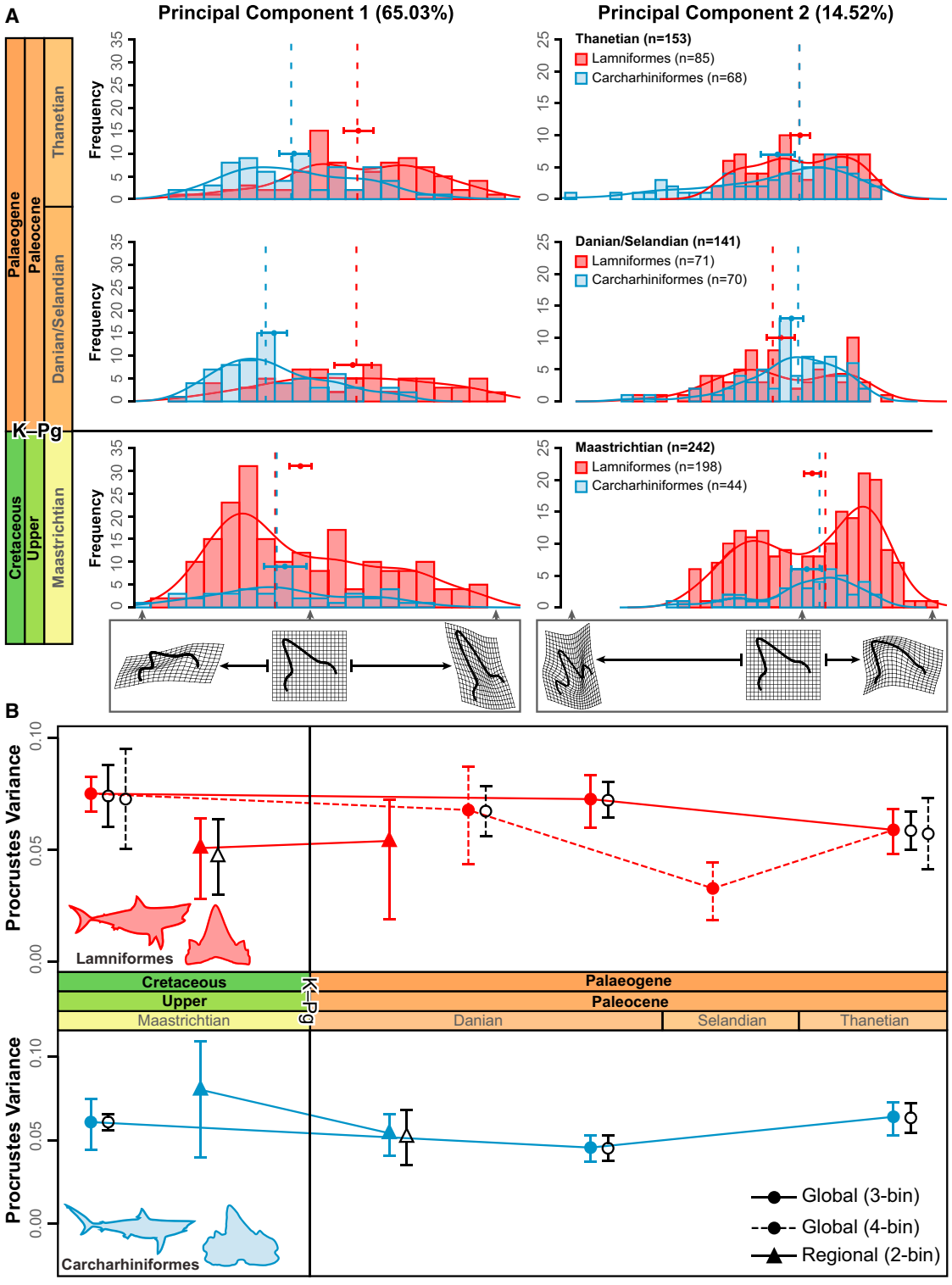

Figure 2. Morphospace and Disparity Dynamics of Lamniform and Carcharhiniform Shark Teeth across the K–Pg Extinction

(A) Histograms of PC1 and PC2 based on the global dataset and three-stage time-binning scheme. Dashed vertical lines indicate median values; points correspond to the arithmetic mean and associated 95% confidence intervals. Proportions of variance described by PC1 and PC2 are given in the plot titles; thin-plate splines correspond to those in Figure 1B.

(B) Disparity trajectories across the K–Pg boundary in lamniforms (top) and carcharhiniforms (bottom). Raw disparity (closed shapes) is shown with 95% confidence intervals calculated from 999 bootstrap pseudoreplicates for each time-bin. Rarefied disparity (open shapes) is shown with 95% prediction intervals of 999 pseudoreplicates subsampled to 50 lamniform and 40 carcharhiniform occurrences (see also Figures S1–S3 and Table S1–S5).

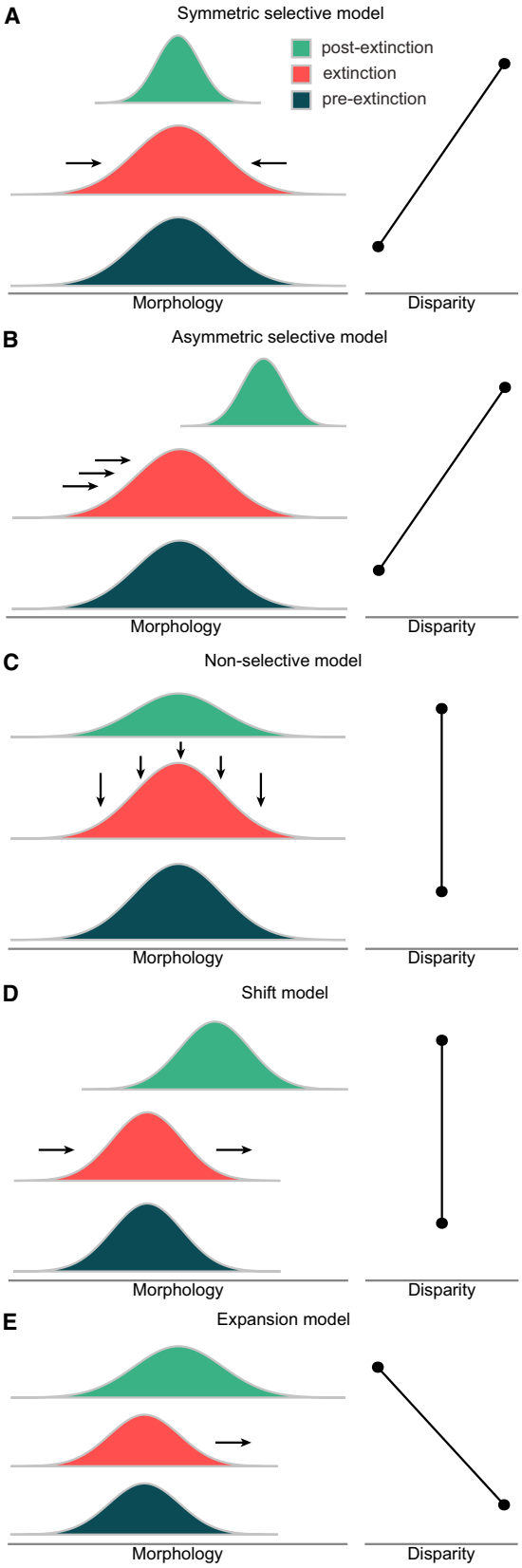

Figure 3. Idealized Morphological Extinction Models

(A–E) Distributions equate to ordinate axes of morphology with associated disparity trajectories from pre- to post-extinction episodes. Arrows indicate the direction of extinction or origination. (A) Symmetric selective model; (B) asymmetric selective model; (C) non-selective model; (D) shift model; and (E) expansion model.

DISCUSSION

Although most often viewed from a terrestrial perspective, the K–Pg mass extinction marked a turning point in the evolutionary history of marine vertebrates. Most conspicuously, oceanic reptilian amniotes almost totally disappeared [5], large-bodied bony fish were severely depleted [3, 4], and teleosts explosively radiated in the early Palaeogene [1, 14]. Despite these major losses among larger-bodied marine carnivores, the survival of sharks suggests that not all higher-trophic-level consumers were affected to the same degree. Sharks, therefore, offer an optimal experimental clade with which to investigate K–Pg extinction and recovery processes and to identify the possible drivers that facilitated their development into modern marine communities.

Extinction and Survival across the K–Pg Boundary

The dynamics of extinctions are usually discussed in terms of selective versus non-selective models [2, 4, 15, 16]. Under a strict selective model, closely related clades are targeted and result in decreased disparity [17]. This scenario predicts a trimming of morphospace, either symmetrically (= no shift in mean morphology but a loss of extreme values [18, 19]; Figure 3A) or asymmetrically (= a shift in mean morphology; Figure 3B). In contrast, a non-selective model (Figure 3C) hypothesizes random extinction across the entire morphological spectrum, with no associated decline in disparity [17] or shift in morphospace. Here, we also consider two additional models: (i) a shift model, which predicts selective extinction of certain morphologies and a corresponding expansion into new regions of morphospace (this produces a shift in mean morphology but no disparity decline: Figure 3D); and (ii) an expansion model, whereby disparity increases in association with the invasion of new morphospace (Figure 3E). The latter is equivalent to an adaptive radiation [20] involving the repopulation of vacant ecological niches.

Our results reveal that the pattern of changing lamniform and carcharhiniform disparity across the K–Pg boundary was almost static and thus superficially fits a non-selective extinction model [17]. This scenario concurs with existing measures of ichthyolith abundance, which suggest that elasmobranchs broadly maintained pre-extinction frequencies well into the earliest Paleocene [14]. Conversely, some regional, albeit insignificant, declines were found to have affected carcharhiniform disparity within our subsample from Stevns Klint. This is contrary to previous studies that otherwise report stagnant taxonomic richness [21]. We attribute such discrepancies to uneven sampling across morphologically uniform (low kurtosis) latest Maastrichtian assemblages versus those from the Danian that are much more condensed (high kurtosis). Of greater importance, however, is our evidence for static global disparity, which deviates from current estimates of moderate genus-level extinctions (between

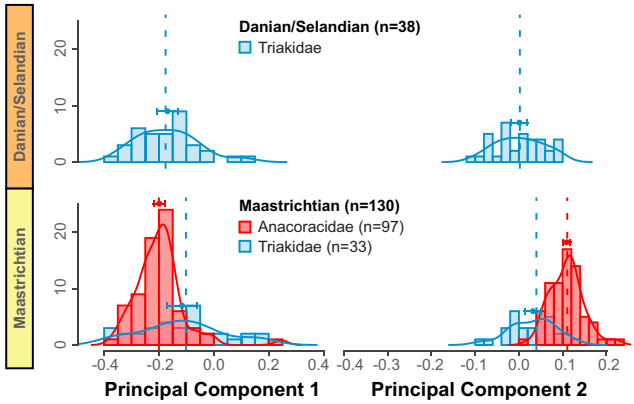

Figure 4. Morphospace Dynamics of Anacoracid and Triakid Shark Teeth across the K–Pg Extinction.

Histograms of PC1 and PC2 showing the distribution of anacoracid (red) and triakid (blue) dental morphologies on a global scale. Dashed vertical lines indicate the median values; points correspond to the arithmetic mean and associated 95% confidence intervals.

27%–34% globally and regionally, respectively) among all sharks across the K–Pg interval [3, 12, 21]. A comparatively minimal decline (4%) has been suggested for carcharhiniforms [11] and is similar to our findings but prompts the conclusion that the morphological and taxonomic turnovers evident in sharks at the end of the Cretaceous were decoupled, much like those reported for other major vertebrate groups traversing the end-Permian [22], Triassic–Jurassic [23], and K–Pg [15] mass extinctions. Such discordance also implies continuous exploration of morphospace and conforms to a simple non-selective model (Figure 3C [17]), yet we posit that there was substantially greater intricacy.

The lamniform dental morphologies most impacted by the K–Pg extinction include those possessing distally curved low-crowned and/or triangular teeth. Narrow and tall-crowned tooth morphotypes were comparatively unaffected [24]. This accords with a strict selective extinction model that continued into the Thanetian with no signs of recovery. The K–Pg transition thus had a prolonged, asymmetrical effect on lamniforms (Figure 2A), which is contrary to previous suggestions for a subsequent replacement by closely related taxa [11]. The most severely affected lamniform dental morphotypes [13] belong to the ubiquitous Cretaceous anacoracids [11, 12] (Figure 4). However, the predictions of a strict selective model are inconsistent with our observed static disparity following their extinction (Figure 2B). We attribute this to the following: (i) a remnant Paleocene survival of other lamniforms bearing low-crowned, triangular teeth; and (ii) selective targeting of anterior tooth positions within the heterodont morphospace of certain anacoracids (these undergo a decline in disparity across the K–Pg interval but are otherwise only minor contributors to the overall disparity signal from our global sample; see discussion in Data Dryad Supplemental File 1; https://doi.org/10.5061/dryad.k30c2n0). Based on such interpretations, we propose a combination of selective and non-selective mechanisms to resolve our seemingly contrasting results.

On the other hand, carcharhiniforms uninterruptedly occupied similar morphospace ranges throughout the Maastrichtian–Thanetian. Yet, there is an abrupt increase in low-crowned (cutting) teeth following the K–Pg extinction—a region of morphospace previously dominated by lamniforms (Figure 2A). Post-extinction carcharhiniforms with cutting teeth are epitomized by triakids (Hound sharks), which diversified taxonomically during the Danian [11, 25]. Our analyses show that triakids occupy morphospace immediately proximal to Cretaceous anacoracids along our PC1, but less so on PC2 (Figure 4). Nevertheless, these two clades are not ecologically equivalent, and carcharhiniform disparity does not increase across the extinction event (Figure 2B). We, therefore, refrain from pre-emptively interpreting the Danian triakid diversification as an adaptive radiation and would rather prefer to consider the possible influence of alternative factors such as prey availability and trophic cascades.

The Origins of Modern Shark Assemblages

Characterizing the ecological significance of temporal shifts in shark dental morphospace is complicated by the "many-to-one mapping dilemma", which describes how one biological structure can have multiple functions or how a single function can be performed by multiple structures [26]. Biomechanical analyses have additionally shown that shark dentitions produce complex and occasionally conflicting functional signals [27–29], implying that the precise ecological relationship between tooth shape and diet is currently underexplored. We therefore deem it pragmatic to consider feeding ecology as only a component within the more elaborate mechanism of shark extinction and recovery during the K–Pg interval. Furthermore, our study exclusively considers biotic factors, but we fully acknowledge that abiotic influences such as temperature and sea level likely played direct, although presently unquantified, roles. Given these constraints, low-crowned, triangular toothed anacoracid lamniforms (e.g., *Squalicorax pristodontus*) have been directly compared to the modern Tiger shark (*Galeocerdo cuvier*) [30] and White shark (*Carcharodon carcharias*) [24]. These extant analogs are apex predators with raptorial dentitions [31–33] capable of processing a wide variety of prey items (= polyphagy), including crustaceans, cephalopods, bony fish, and marine amniotes [34, 35] (notably, the White shark can also exhibit ontogeny and size-related specialization for feeding on marine mammals [36]). Approximately equivalent diets may, therefore, be inferred for at least some anacoracids. However, the selective extinction of these particular sharks, as demonstrated by our results, suggests that smaller teleost fishes (e.g., acanthomorphs, which radiated during the earliest Palaeogene [1]) were probably not a primary food source for most members of this clade. Instead, our morphospace classification of anacoracids hints at a dietary repertoire potentially incorporating cephalopods, marine amniotes, and/or larger-bodied bony fish. These groups all underwent sudden ecological collapse at the K–Pg boundary [4–6], which in turn could have contributed to the selective extinction of associated dental morphologies from the recovering spectrum of lamniform shark disparity.

A direct causal relationship between the decline of Cretaceous anacoracids, and subsequent increase of Paleocene triakids, cannot be established from our data. Triakids are nectobenthic hunters of fish and invertebrates that possess heterogeneous dentitions capable of clutching, cutting, and crushing [37]. Substantial differences in their tooth morphology (visible along our

PC2), together with much smaller body sizes ($\leq$2 m) relative to most anacoracids, reflect contrasting ecologies. Consequently, we reject a simple extinction-replacement scenario. Rather, the depletion of certain lamniform morphologies (and possible ecologies) at the end of the Cretaceous [4, 38] and the diversification of triakids, in conjunction with other middle-level consumers, conforms to the tenets of a top-down trophic cascade, whereby extinctions at the apex of the food chain trigger a ''mesopredator release'' [39, 40]. Alternatively, the rapid diversification of teleosts [1, 14] might have prompted a correlated shift at higher trophic levels that was filled by triakids, but these scenarios are not mutually exclusive, and both mechanisms could certainly have contributed to the success of carcharhiniforms after the K–Pg event. As a relevant parallel, it is worth noting that the elimination of apex predators by chronic overfishing has produced similar effects among modern sharks [39].

Regardless of the specific mechanisms, the attenuation of particular lamniform dental morphologies and the subsequent proliferation of similar carcharhiniform tooth structures after the end of the Cretaceous marks an important change in the compositional aspect of selachimorph assemblages. A comparable alteration is also evidenced by taxic abundance, which shows that lamniforms generally dominated late Cretaceous shark faunas, while carcharhiniform diversity was relatively low [11]. In contrast, carcharhiniforms constitute the largest order of extant sharks with over 250 species, and substantially outnumber lamniforms, which are represented by only 15 species [41]. Previous studies have calibrated this turnover with the late Eocene proliferation of reef fishes [7–10, 42–44], although, our results reveal that the foundations were probably laid during the K–Pg event. We also fundamentally dismiss assertions that the K–Pg transition had a limited overall evolutionary impact on the radiation of selachimorphs [14], and would alternatively underscore its pivotal role in shaping the biodiversity and ecosystem complexity that is expressed in the shark communities of today.

STAR★METHODS

Detailed methods are provided in the online version of this paper and include the following:

- KEY RESOURCES TABLE
- CONTACT FOR REAGENT AND RESOURCE SHARING
- EXPERIMENTAL MODEL AND SUBJECT DETAILS
  - Philosophical Rationale
  - Taxonomic Scope and Dataset Assembly
  - Stratigraphic Conventions
- METHOD DETAILS
  - Geometric Morphometric Analyses
- QUANTIFICATION AND STATISTICAL ANALYSIS
  - Disparity and Morphospace Analyses
  - Sensitivity Analyses
- DATA AND SOFTWARE AVAILABILITY

SUPPLEMENTAL INFORMATION

Supplementary information includes three figures and five tables and can be found with this article online at https://doi.org/10.1016/j.cub.2018.05.093.

ACKNOWLEDGMENTS

Mikael Siversson (Western Australian Museum), David Ward (The Natural History Museum), Illiam Jackson (Lund University), Dean Adams (Iowa State University), Jesper Milan (Geomuseum Faxe), Akinobu Watanabe (University College London), Kevin Seymour (Royal Ontario Museum), and Merve Öztoprak (University of Göttingen) are thanked for information and discussions. Thomas Reinecke (Bochum, Germany) provided important image data. Finally, special thanks to three anonymous reviewers who provided good comments that improved the manuscript. The Royal Swedish Academy of Sciences (GS2017-0018) to M.B. and a Wallenberg Scholarship from the Knut and Alice Wallenberg Foundation to P.E.A. funded our research.

AUTHOR CONTRIBUTIONS

M.B. and N.E.C. designed the study, collected and analyzed the data, interpreted the results, and wrote the manuscript. B.P.K. interpreted the results and wrote the manuscript. B.P.K., H.B., and P.E.A. conceived the project. All authors were involved in discussing the results and revising the manuscript.

DECLARATION OF INTERESTS

The authors declare no competing interests.

Received: February 12, 2018
Revised: April 5, 2018
Accepted: May 31, 2018
Published: August 2, 2018

REFERENCES

1. Friedman, M. (2010). Explosive morphological diversification of spiny-finned teleost fishes in the aftermath of the end-Cretaceous extinction. P. Roy. Soc. B-Biol. Sci. *277*, 1675–1683.
2. Wilson, G.P. (2013). Mammals across the K/Pg boundary in northeastern Montana, U.S.A.: dental morphology and body-size patterns reveal extinction selectivity and immigrant-fueled ecospace filling. Paleobiology *39*, 429–469.
3. Friedman, M., and Sallan, L.C. (2012). Five hundred million years of extinction and recovery: a Phanerozoic survey of large-scale diversity patterns in fishes. Palaeontology *55*, 707–742.
4. Friedman, M. (2009). Ecomorphological selectivity among marine teleost fishes during the end-Cretaceous extinction. Proc. Natl. Acad. Sci. USA *106*, 5218–5223.
5. Benson, R.B.J., and Butler, R.J. (2011). Uncovering the diversification history of marine tetrapods: ecology influences the effect of geological sampling biases. Geol. Soc. Lond. Spec. Publ. *358*, 191–208.
6. MacLeod, N., Rawson, P.F., Forey, P.L., Banner, F.T., Boudagher-Fadel, M.K., Bown, P.R., Burnett, J.A., Chambers, P., Culver, S., Evans, S.E., et al. (1997). The Cretaceous-Tertiary biotic transition. J. Geol. Soc. *154*, 265–292.
7. Adnet, S., Antoine, P.-O., Hassan Baqri, S.R., Crochet, J.-Y., Marivaux, L., Welcomme, J.-L., and Métais, G. (2007). New tropical carcharhinids (Chondrichthyes, Carcharhiniformes) from the late Eocene–early Oligocene of Balochistan, Pakistan: Paleoenvironmental and paleogeographic implications. J. Asian Earth Sci. *30*, 303–323.
8. Iserbyt, A., and De Schutter, P.J. (2012). Quantitative analysis of Elasmobranch assemblages from two successive Ypresian (early Eocene) facies at Marke, western Belgium. Geol. Belg. *15*, 146–153.
9. Underwood, C.J., Ward, D.J., King, C., Antar, S.M., Zalmout, I.S., and Gingerich, P.D. (2011). Shark and ray faunas in the Middle and Late Eocene of the Fayum Area, Egypt. P. Geologist. Assoc. *122*, 47–66.
10. Sorenson, L., Santini, F., and Alfaro, M.E. (2014). The effect of habitat on modern shark diversification. J. Evol. Biol. *27*, 1536–1548.

11. Guinot, G., and Cavin, L. (2016). 'Fish' (Actinopterygii and Elasmobranchii) diversification patterns through deep time. Biol. Rev. Camb. Philos. Soc. *91*, 950–981.
12. Kriwet, J., and Benton, M.J. (2004). Neoselachian (Chondrichthyes, Elasmobranchii) diversity across the Cretaceous–Tertiary boundary. Palaeogeogr. Palaeoclimatol. Palaeoecol. *214*, 181–194.
13. Cappetta, H. (2012). Chondrichthyes—Mesozoic and Cenozoic Elasmobranchii: teeth (München: Verlag F. Pfeil).
14. Sibert, E.C., and Norris, R.D. (2015). New Age of Fishes initiated by the Cretaceous-Paleogene mass extinction. Proc. Natl. Acad. Sci. USA *112*, 8537–8542.
15. Grossnickle, D.M., and Newham, E. (2016). Therian mammals experience an ecomorphological radiation during the Late Cretaceous and selective extinction at the K–Pg boundary. P. Roy. Soc. B-Biol. Sci. *283*, 20160256.
16. Jablonski, D. (2005). Mass extinctions and macroevolution. Paleobiology *31*, 192–210.
17. Foote, M. (1993). Discordance and concordance between morphological and taxonomic diversity. Paleobiology *19*, 185–204.
18. Simon, M.S., Korn, D., and Koenemann, S. (2010). Disparity fluctuations in Jurassic ammonoids by means of conch geometry. Palaeogeogr. Palaeoclimatol. Palaeoecol. *292*, 520–531.
19. Korn, D., Hopkins, M.J., and Walton, S.A. (2013). Extinction space–a method for the quantification and classification of changes in morpho-space across extinction boundaries. Evolution *67*, 2795–2810.
20. Simpson, G.G. (1953). The Major Features of Evolution (New York: Columbia University Press).
21. Adolfssen, J.S., and Ward, D.J. (2014). Crossing the boundary: an elasmobranch fauna from Stevns Klint, Denmark. Palaeontology *57*, 591–629.
22. Ruta, M., Angielczyk, K.D., Fröbisch, J., and Benton, M.J. (2013). Decoupling of morphological disparity and taxic diversity during the adaptive radiation of anomodont therapsids. P. Roy. Soc. B-Biol. Sci. *280*, 20131071.
23. Brusatte, S.L., Benton, M.J., Ruta, M., and Lloyd, G.T. (2008). The first 50Myr of dinosaur evolution: macroevolutionary pattern and morphological disparity. Biol. Lett. *4*, 733–736.
24. Belben, R.A., Underwood, C.J., Johanson, Z., and Twitchett, R.J. (2017). Ecological impact of the end-Cretaceous extinction on lamniform sharks. PLoS ONE *12*, e0178294.
25. Maisey, J.G. (2012). What is an 'elasmobranch'? The impact of palaeontology in understanding elasmobranch phylogeny and evolution. J. Fish Biol. *80*, 918–951.
26. Wainwright, P.C., Alfaro, M.E., Bolnick, D.I., and Hulsey, C.D. (2005). Many-to-One Mapping of Form to Function: A General Principle in Organismal Design? Integr. Comp. Biol. *45*, 256–262.
27. Bergman, J.N., Lajeunesse, M.J., and Motta, P.J. (2017). Teeth penetration force of the tiger shark *Galeocerdo cuvier* and sandbar shark *Carcharhinus plumbeus*. J. Fish Biol. *91*, 460–472.
28. Huber, D.R., Claes, J.M., Mallefet, J., and Herrel, A. (2009). Is extreme bite performance associated with extreme morphologies in sharks? Physiol. Biochem. Zool. *82*, 20–28.
29. Whitenack, L.B., and Motta, P.J. (2010). Performance of shark teeth during puncture and draw: implications for the mechanics of cutting. Biol. J. Linn. Soc. Lond. *100*, 271–286.
30. Shimada, K., and Cicimurri, D.J. (2005). Skeletal anatomy of the Late Cretaceous shark, Squalicorax (Neoselachii: Anacoracidae). Paläont. Z. *79*, 241–261.
31. Compagno, L.J.V. (1990). Relationships of the megamouth shark, *Megachasma pelagios* (Lamniformes: Megachasmidae), with comments on its feeding habits. NOAA Nat. Mar. Fish. Serv. *90*, 357–379.
32. Meyer, C.G., O'Malley, J.M., Papastamatiou, Y.P., Dale, J.J., Hutchinson, M.R., Anderson, J.M., Royer, M.A., and Holland, K.N. (2014). Growth and maximum size of tiger sharks (*Galeocerdo cuvier*) in Hawaii. PLoS ONE *9*, e84799.
33. Burgess, G.H., Bruce, B.D., Cailliet, G.M., Goldman, K.J., Grubbs, R.D., Lowe, C.G., MacNeil, M.A., Mollet, H.F., Weng, K.C., and O'Sullivan, J.B. (2014). A re-evaluation of the size of the white shark (Carcharodon carcharias) population off California, USA. PLoS ONE *9*, e98078.
34. Cortés, E. (1999). Standardized diet compositions and trophic levels of sharks. ICES J. Mar. Sci. *56*, 707–717.
35. Dicken, M.L., Hussey, N.E., Christiansen, H.M., Smale, M.J., Nkabi, N., Cliff, G., and Wintner, S.P. (2017). Diet and trophic ecology of the tiger shark (*Galeocerdo cuvier*) from South African waters. PLoS ONE *12*, e0177897.
36. Hussey, N.E., McCann, H.M., Cliff, G., Dudley, S.F.J., Wintner, S.P., and Fisk, A.T. (2012). Size-based analysis of diet and trophic position of the White Shark, *Carcharodon carcharias*. In South African waters. In Global Perspectives on the Biology and Life History of the White Shark, M.L. Domeier, ed. (Boca Raton: CRC Press), pp. 27–49.
37. Compagno, L.J.V. (1984). FAO species catalogue, volume 4. Sharks of the world: an annotated and illustrated catalogue of shark species known to date. Part 2. Carcharhiniformes. FAO Fish *125*, 251–655.
38. Bardet, N. (1994). Extinction events among Mesozoic marine reptiles. Hist. Biol. *7*, 313–324.
39. Myers, R.A., Baum, J.K., Shepherd, T.D., Powers, S.P., and Peterson, C.H. (2007). Cascading effects of the loss of apex predatory sharks from a coastal ocean. Science *315*, 1846–1850.
40. Estes, J.A., Terborgh, J., Brashares, J.S., Power, M.E., Berger, J., Bond, W.J., Carpenter, S.R., Essington, T.E., Holt, R.D., Jackson, J.B.C., et al. (2011). Trophic downgrading of planet Earth. Science *333*, 301–306.
41. Compagno, L.J.V. (2005). Checklist of living Chondrichthyes. In Reproductive Biology and Phylogeny of Chondrichthyes: Sharks, Batoids and Chimaeras, *Volume 3*, W.C. Hamlet, ed. (Enfield: Science Publishes, Inc.), pp. 501–548.
42. Alfaro, M.E., Santini, F., and Brock, C.D. (2007). Do reefs drive diversification in marine teleosts? Evidence from the pufferfishes and their allies (Order Tetraodontiformes). Evolution *61*, 2104–2126.
43. Cowman, P.F., and Bellwood, D.R. (2013). The historical biogeography of coral reef fishes: global patterns of origination and dispersal. J. Biogeogr. *40*, 209–224.
44. Santini, F., Nguyen, M.T.T., Sorenson, L., Waltzek, T.B., Lynch Alfaro, J.W., Eastman, J.M., and Alfaro, M.E. (2013). Do habitat shifts drive diversification in teleost fishes? An example from the pufferfishes (Tetraodontidae). J. Evol. Biol. *26*, 1003–1018.
45. Rohlf, F.J. (2017). TpsDig2, Version 2.3 (Stony Brook: Published by the Author).
46. R Development Core Team (2017). R: a language and environment for statistical computing, Version 3.3.3 (Vienna: R Foundation for Statistical Computing).
47. Guinot, G., Adnet, S., and Cappetta, H. (2012). An analytical approach for estimating fossil record and diversification events in sharks, skates and rays. PLoS ONE *7*, e44632.
48. Kriwet, J., Kiessling, W., and Klug, S. (2009). Diversification trajectories and evolutionary life-history traits in early sharks and batoids. P. Roy. Soc. B-Biol. Sci. *276*, 945–951.
49. Alroy, J., Aberhan, M., Bottjer, D.J., Foote, M., Fürsich, F.T., Harries, P.J., Hendy, A.J.W., Holland, S.M., Ivany, L.C., Kiessling, W., et al. (2008). Phanerozoic trends in the global diversity of marine invertebrates. Science *321*, 97–100.
50. Adams, D.C., and Otárola-Castillo, E. (2013). geomorph: an r package for the collection and analysis of geometric morphometric shape data. Methods Ecol. Evol. *4*, 393–399.
51. Foote, M. (1993). Contributions of individual taxa to overall morphological disparity. Paleobiology *19*, 403–419.
52. Foote, M. (1997). The evolution of morphological diversity. Annu. Rev. Ecol. Syst. *28*, 129–152.

53. Foote, M. (1991). Morphological and taxonomic diversity in clade's history: the blastoid record and stochastic simulations. Contrib. Mus. Geol. U. Mich. *28*, 101–140.

54. Bookstein, F.L. (1991). Morphometric Tools for Landmark Data: Geometry and Biology (Cambridge: Cambridge University Press).

55. Collyer, M.L., Sekora, D.J., and Adams, D.C. (2015). A method for analysis of phenotypic change for phenotypes described by high-dimensional data. Heredity (Edinb) *115*, 357–365.

56. Benjamini, Y., and Hochberg, Y. (1995). Controlling the false discovery rate: a practical and powerful approach to multiple testing. J. Roy. Stat. Soc. Series B Met. *57*, 289–300.

57. Ciampaglio, C.N., Kemp, M., and McShea, D.W. (2001). Detecting changes in morphospace occupation patterns in the fossil record: characterization and analysis of measures of disparity. Paleobiology *27*, 695–715.

58. Zelditch, M.L., Swiderski, D.L., Sheets, H.D., and Fink, W.L. (2004). Geometric Morphometrics for Biologists: A Primer (London: Academic Press).

59. Sanders, H.L. (1968). Marine Benthic Diversity: A Comparative Study. Am. Nat. *102*, 243–282.

60. Foote, M. (1992). Rarefaction analysis of morphological and taxonomic diversity. Paleobiology *18*, 1–16.

61. Mannering, A.A., and Hiller, N. (2008). An early Cenozoic neoselachian shark fauna from the Southwest Pacific. Palaeontology *51*, 1341–1365.

62. Cappetta, H., and Nolf, D. (2005). Révision de quelques Odontaspididae (Neoselachii: Lamniformes) du Paléocène et de l'Eocène du Bassin de la mer du Nord. Bull. Inst. R. Sn. N. B.-S. *75*, 237–266.

63. Underwood, C.J., and Ward, D.J. (2008). Sharks of the order Carcharhiniformes from the British Coniacian, Santonian and Campanian (Upper Cretaceous). Palaeontology *51*, 509–536.

STAR★METHODS

KEY RESOURCES TABLE

REAGENT or RESOURCE	SOURCE	IDENTIFIER
Deposited Data		
Supplementary results and methods	This paper	Data Dryad Supplemental File 1; https://doi.org/10.5061/dryad.k30c2n0
Morphometric data sources	This paper	Data Dryad Supplemental File 2; https://doi.org/10.5061/dryad.k30c2n0
Landmark coordinate data	This paper	Data Dryad Supplemental File 3; https://doi.org/10.5061/dryad.k30c2n0
Sliders file	This paper	Data Dryad Supplemental File 4; https://doi.org/10.5061/dryad.k30c2n0
R source code	This paper	R Scripts; https://doi.org/10.5061/dryad.k30c2n0
Software and Algorithms		
tpsDig2	[45]	http://life.bio.sunysb.edu/morph/soft-dataacq.html
R	[46]	https://www.r-project.org/

CONTACT FOR REAGENT AND RESOURCE SHARING

Further information and requests for resources (R scripts, raw image data) should be directed to and will be fulfilled by the Lead Contact, Mohamad Bazzi (mohamad.bazzi@ebc.uu.se).

EXPERIMENTAL MODEL AND SUBJECT DETAILS

Philosophical Rationale

Taxonomic richness has historically formed the basis for reconstructing palaeobiodiversity in sharks [11, 12, 47, 48]. However, the use of raw genus or species-level counts is problematic when dealing with an anatomically incomplete selachimorph fossil record with recognized preservational and sampling biases toward isolated teeth [48, 49]. Moreover, subjective differences in taxonomic philosophies ('lumping' versus 'splitting') add a level of untestable ambiguity to measures of palaeobiodiversity. As a result, our study adopts the Procrustes paradigm [50] to investigate temporal patterns of occupation and disparity within dental morphospace. Disparity provides a quantitative measure that is independent of taxonomic assignments [17, 51, 52]. Its frequent decoupling from taxonomic richness [53] also provides a reliable indicator of ecology [52], and is thus better suited to reconstructing eco-evolutionary patterns through time. Here we use taxonomy only to delimit the broad comparative groups Lamniformes and Carcharhiniformes, as well as some relevant family-level constituent clades.

Taxonomic Scope and Dataset Assembly

Our complete morphometric dataset encompasses lamniform and carcharhiniform teeth from the Maastrichtian and Paleocene (72–56 Ma). In order to quantify issues associated with uneven geographical sampling, we also analyzed a locality-restricted subsample from Stevns Klint. All of our specimens were sourced from published images including digital photographs and line drawings depicting either lingual or labial views. Published images are a practical means of approximating global-level diversity in sharks, although we acknowledge that they under-represent common teeth. Published images will, nonetheless, emphasize morphological variation and it is therefore unlikely that our results underestimate disparity. The fact that our rarefaction and raw disparity values are virtually identical (Figure 2B) further demonstrates that restricted sampling does not greatly affect overall patterns. As a result, we deem such data to be adequate for interpreting large-scale morphospace shifts, even though they may be of limited use for reconstructing actual numerical abundance.

Stratigraphic Conventions

To assess patterns of disparity across the K–Pg boundary, we time-binned our data into consecutive stage-level intervals: Maastrichtian, Danian, Selandian, and Thanetian. However, some specimens (N = 81, 13.57% of the total global dataset) were of indeterminate Danian or Selandian age, in which case a combined Danian/Selandian bin was allocated. Although this approach generates time-averaging, it ameliorates issues associated with uneven sampling and temporal range differentiation between pre- and post-extinction assemblages. The stratigraphic resolution of the Stevns Klint subsample also permits examination of sub-stage level time-bins for the late Maastrichtian based on the Højerup Member (calcareous nannofossil zonation UC20d) of the Møns Klint Formation, and early Danian Fiskeler (P0), and Cerithium Limestone (Pα) members of the Rødvig Formation [21].

METHOD DETAILS

Geometric Morphometric Analyses

We employed a 2D geometric morphometric approach based on three homologous landmarks (*k*), and 147 sliding semi-landmarks (*s*). Only non-pathological teeth with complete crowns were analyzed and low-resolution images were discarded. In order to standardize orientation, all teeth were positioned such that the tooth apex was directed to the left. Initial digitization was conducted using *tpsDig2* (v. 2.18) [45], after which the tps file was imported into *R* [46] using a customized code that resampled the original *tpsDig2* curves into 150 equidistant landmarks.

QUANTIFICATION AND STATISTICAL ANALYSIS

Disparity and Morphospace Analyses

The digitized data were subjected to a Generalized Procrustes Analysis (GPA) to account for differences in orientation and isometric size variation. Sliding semi-landmarks were optimized using minimized bending energies [54]. The GPA-aligned coordinates formed the basis for subsequent morphospace and disparity analyses. Morphospace was examined via a Principal Component Analysis (PCA) in *geomorph* [51] with default settings and eigenvalues/eigenvectors calculated from the covariance matrix. Overall patterns were interpreted from standard bivariate plots of the PC axes; however, shifts in morphospace through time were visualized using histograms and probability density curves of specific axes of variation (e.g., Figure S1). Significant shifts in morphospace were tested through: (1) a one-way Procrustes analysis of variance, which is equivalent to a nonparametric (np)-MANOVA, and included 999 permutations carried out across all axes of variation [55]; (2) standard confidence intervals of the means; and (3) a two-sampled Kolmogorov–Smirnov (K–S) test. All *a posteriori* pairwise tests (Procrustes ANOVA and K–S tests) were adjusted using the False Discovery Rate (FDR) to limit false positives [56]. Interpretations of morphology along ordinated (scaled) axes are depicted via thin-plate spline deformation grids (TPS).

We employed Procrustes variances (*PV*) to quantify disparity. This metric is variance-based, an approach that is less sensitive to sample size than range-based metrics [51, 57]. PV is equal to the sum of the squared Euclidean distances between GPA-aligned specimens (d_{GPA}), divided by the square of the number of observations (i.e., sample size *N*), and is equivalent to the trace of the covariance matrix divided by the sample size [50, 58].

$$PV = \frac{\sum d_{GPA}^2}{N^2}$$

PVs were calculated for lamniforms and carcharhiniforms separately and plotted across the time-bins for both the total global sample, and regional subsample respectively. Significant differences in disparity between time-bins were examined via: (1) pairwise comparisons using permutation tests implemented in *geomorph* ($N_{iterations} = 999$); and (2) bootstrap confidence intervals ($N_{iterations} = 999$).

In addition, we adopted a rarefaction approach (pseudo-replicated 999 times) to assess the effects of uneven sample sizes between successive time-bins. This standardizes sample sizes in each bin to a predetermined level [59, 60]. Subsampling was carried out down to the lowest sampled time-bin. In the four-stage time binning scheme, the Selandian has the smallest sample size ($N_{Lamniformes} = 23$; $N_{Carcharhiniformes} = 2$), whereas under a three-stage binning scheme the combined Danian/Selandian has the smallest sample ($N_{Lamniformes} = 71$; $N_{Carcharhiniformes} = 70$). Because the Selandian is poorly sampled for carcharhiniforms, we did not interpret this bin in detail, and rather, focused on the combined three-stage binning scheme.

Sensitivity Analyses

We evaluated various confounding factors relevant for fossil-based time-series analyses including geographic sampling, sampling techniques, and monognathic heterodonty.

Our dataset geographically includes fossils from continental Europe, North America, and North Africa (Figure 1A). Specimens from Asia and Antarctica were only recorded from the Maastrichtian, whereas samples from Oceania represent only the Danian/Selandian [61]. Geographic sampling bias is most marked during the Danian, where 38.3% (N = 54) of our sample derives from Stevns Klint [21]. Selandian sampling is likewise confined to the Maret locality in Belgium [62]. We accommodated geographic sampling limitations for our global dataset via: (1) analyzing the Stevns Klint subsample separately (Figure S2); and (2) analyzing the total global sample with the Stevns Klint subsample excluded (Figure S3).

We also anticipate that our global sample might be biased by field collecting techniques, with larger, more visibly conspicuous teeth being easier to obtain from surface outcrop, as opposed to smaller teeth that require labor-intensive bulk sampling [63]. This could potentially result in an under-representation of particular lineages, and a deficient sampling artifact that is unreflective of genuine biodiversity trends. To counter, we specifically selected the Stevns Klint subsample to confirm our signals because this geographically constrained locality was systematically excavated using a comprehensive bed-by-bed bulk sampling survey [21].

Selachimorph dentitions are known to exhibit heterodonty, including monognathic variation along a tooth row, and dignathic variation between the upper and lower jaws [13]. These conditions may influence patterns in morphospace but would be difficult to discriminate using isolated teeth. The effects of monognathic heterodonty were therefore tested via: (1) grouping alternate subsamples of anterior versus lateroposterior teeth; (2) determining significant differences in disparity among tooth positions in morphospace; and (3) visually inspecting the distribution of tooth positions along specific axes of variation. Unfortunately, the current dataset

is insufficient to determine the effects of dignathic heterodonty. Nevertheless, we recovered a significant decline in lamniform disparity when only anterior teeth were considered. This is based on a small subsample of the global dataset but suggests that a shift in monognathic heterodonty occurred across the K–Pg interval. Furthermore, it is driven by the loss of anacoracids, whose anterior teeth load negatively along our PC1, and thus conforms to the overall asymmetric selective extinction pattern evident in our morphospace dynamics (Figures 2A and 4).

DATA AND SOFTWARE AVAILABILITY

Additional information and test results, together with our occurrence and morphometric datasets, and the R scripts are archived at the Dryad Digital Repository (https://doi.org/10.5061/dryad.k30c2n0).

Current Biology, Volume *28*

Supplemental Information

Static Dental Disparity and Morphological Turnover in Sharks across the End-Cretaceous Mass Extinction

Mohamad Bazzi, Benjamin P. Kear, Henning Blom, Per E. Ahlberg, and Nicolás E. Campione

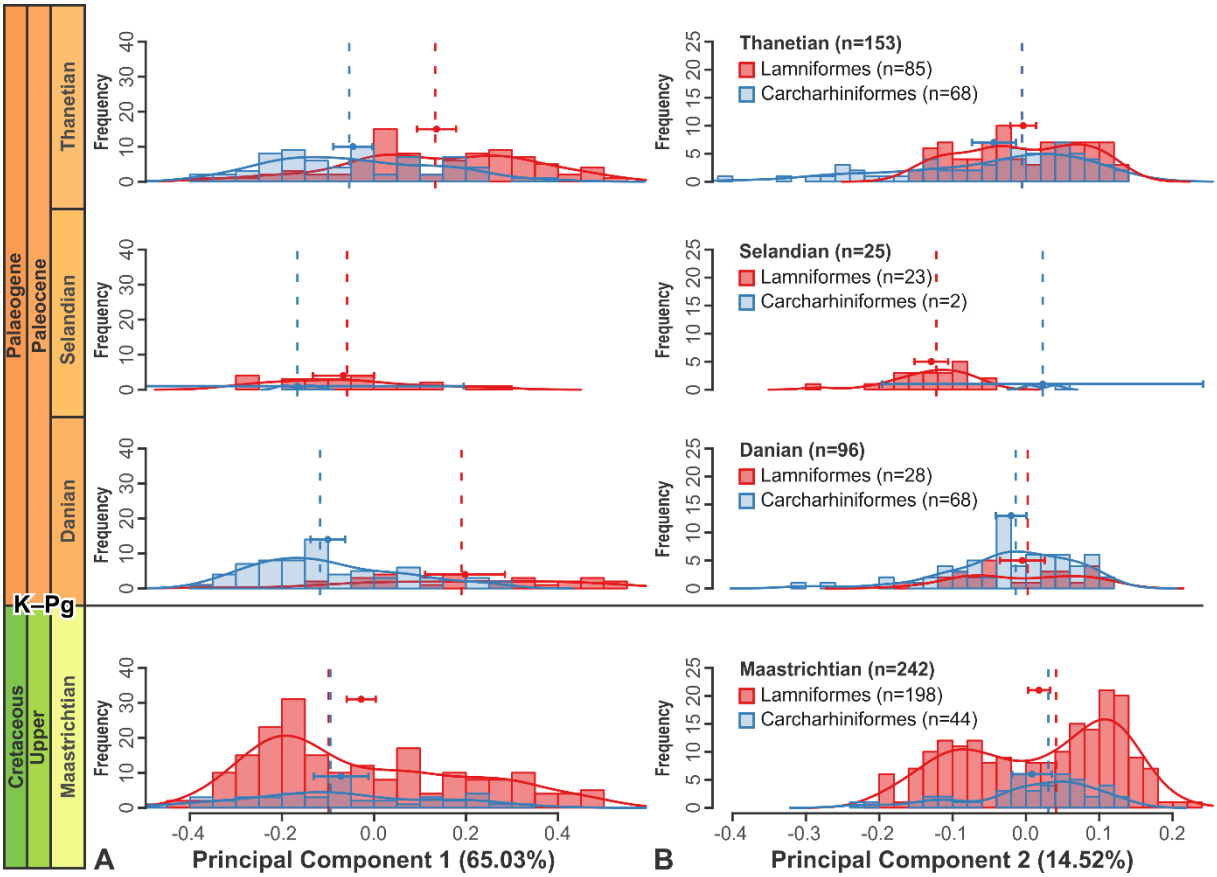

Figure S1. Global temporal patterns in morphospace. Related to the main text, Figure 2A and the STAR ★ Methods. Histograms show the distribution of dental morphologies in lamniforms (red) and carcharhiniforms (blue) along **(A)** PC1, and **(B)** PC2 on a global scale using the four-stage time binning scheme. Dashed vertical lines indicate median values; points correspond to arithmetic mean and associated 95% confidence intervals. Proportion of variance described by PC1 and PC2 are given in the axis labels.

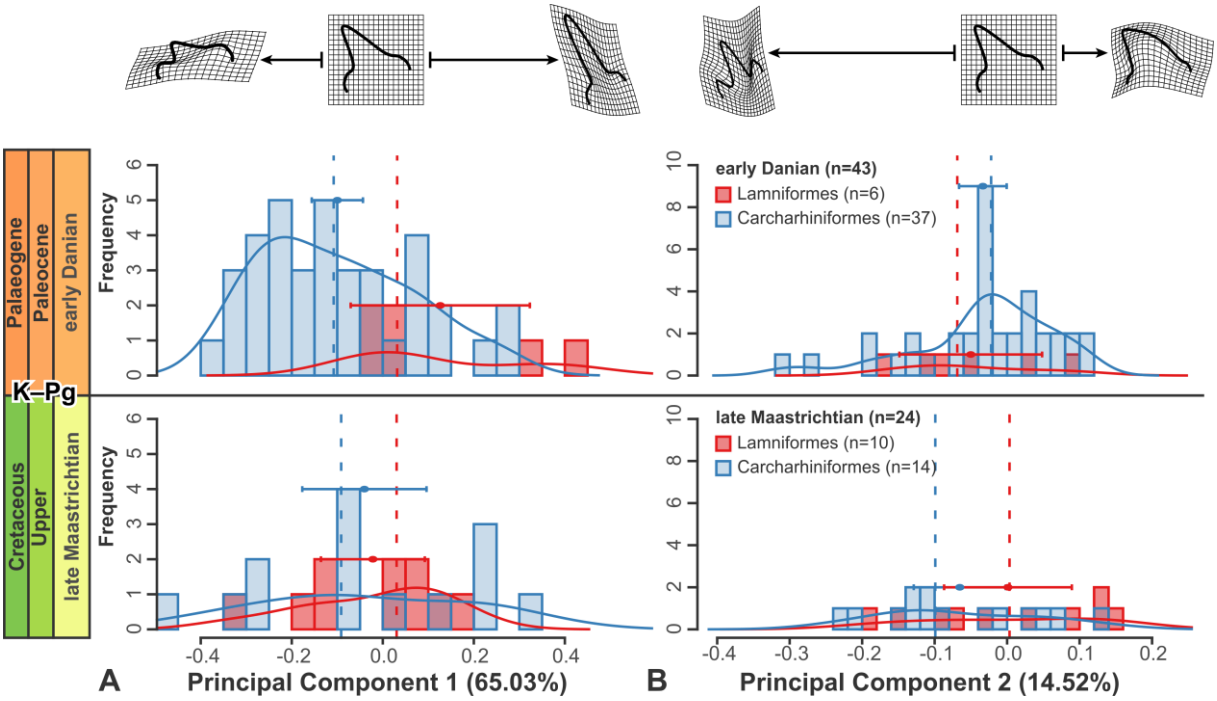

Figure S2. Regional temporal patterns in morphospace. Related to the main text, Figure 2A and the STAR ★ Methods. Histograms show the distribution of dental morphologies (thin-plate spline deformation grids at top) in lamniforms (red) and carcharhiniforms (blue) along **(A)** PC1, and **(B)** PC2, based on the regional subsample from Stevns Klint. Dashed vertical lines indicate median values; points correspond to the arithmetic mean and associated 95% confidence intervals. Proportion of variance described by PC1 and PC2 are given in the axis labels.

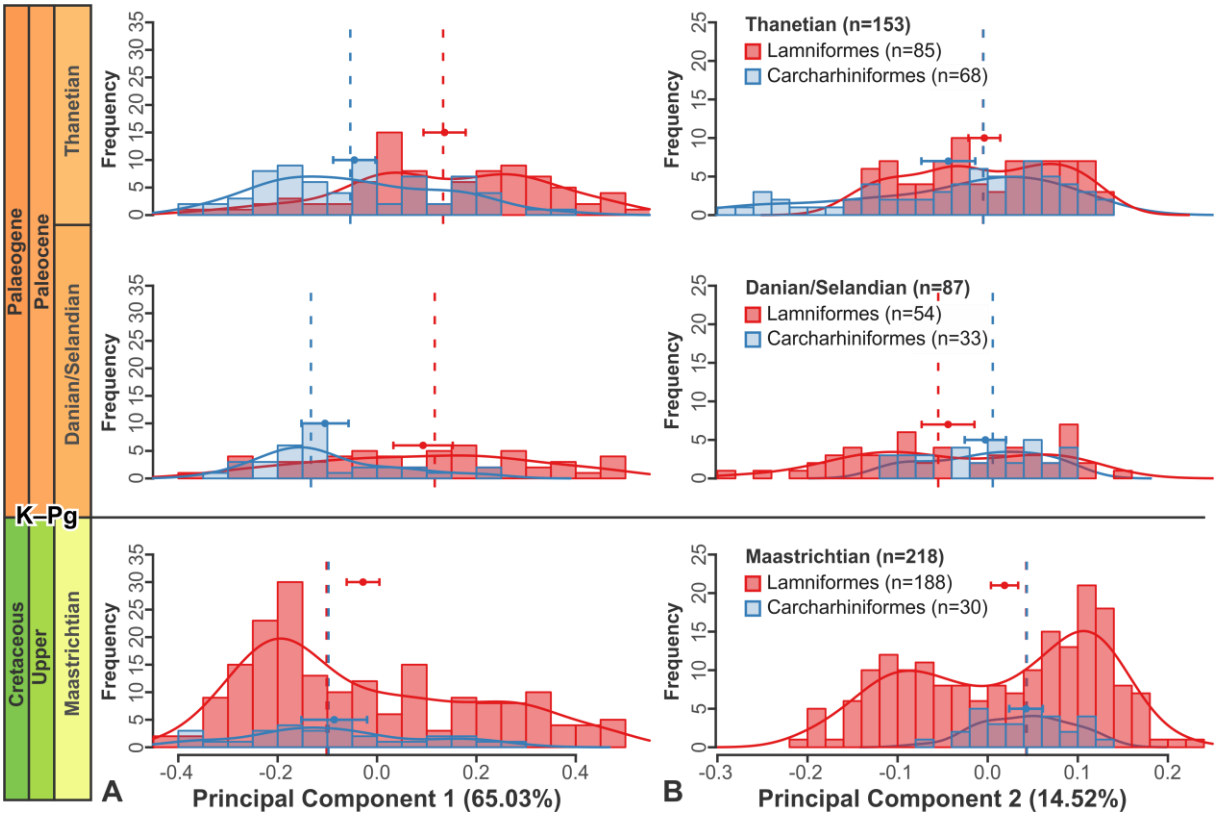

Figure S3. Testing exclusion of the regional subsample from Stevns Klint to validate global patterns of morphospace occupation. Related to the main text, Figure 2A and the STAR ★ Methods. Histograms show the distribution of dental morphologies in lamniforms (red) and carcharhiniforms (blue) along **(A)** PC1, and **(B)** PC2 on a global scale using the three-stage binning scheme. Dashed vertical lines indicate median values; points correspond to the arithmetic mean and associated 95% confidence intervals. Proportion of variance described by PC1 and PC2 are given in the axis labels.

Principal Component ($u_{k)}$	Standard Deviation (σ)	Proportion of Variance (%)	Cumulative Proportion
PC1	0.2208	65.03	0.6503
PC2	0.1044	14.52	0.7956
PC3	0.07105	6.731	0.86289
PC4	0.05499	4.032	0.90321
PC5	0.04229	2.385	0.92706
PC6	0.03380	1.523	0.94230
PC7	0.02784	1.033	0.95263
PC8	0.02548	0.866	0.96129
PC9	0.02269	0.686	0.96815
PC10	0.01815	0.439	0.97254

Table S1. Computed variance (eigenvalues, λ_k) explained by the first 10 principal component (PCA) axes (eigenvectors, u_k). Related to Figures 1B and 2. Number of components generated by the PCA amounts to 300.

np-MANOVA	*d.f.*	SSE	SS	R^2	F	Z	Pr(>F)
Lamniformes							
Global (four-bin analysis)	330	22.536	3.3156	0.12826	16.184	5.2536	0.001**
Global (three-bin analysis)	351	25.045	2.5025	0.090845	17.536	4.5987	0.001**
Regional (two-bin analysis)	14	0.83149	0.10716	0.11416	1.8043	1.1245	1.145
Carcharhiniformes							
Global (four-bin analysis)	178	10.200	0.30806	0.029316	1.792	1.4434	0.082
Global (three-bin analysis)	179	10.220	0.28819	0.027426	2.5238	1.8473	0.034*
Carcharhiniformes (two-bin analysis)	49	3.1265	0.061206	0.019201	0.9593	0.40227	0.349

Table S2. Nonparametric multivariate analysis of variance (np-MANOVA). Related to Figure 2A, Figures S1 and S2. Symbols/Abbreviations: *d.f.* = degrees of freedom; SSE = Error Sum of Squares; SS = sequential sums of squares; F statistics = F value by permutation; R^2 = partial R-squared; Z = effect size. P-values are based on 999 permutations. **denotes significant results ($p<0.05$).

	Maastrichtian				Danian/Selandian				Thanetian			
All Axes	L		C		L		C		L		C	
Maastrichtian					**0.001**		0.116		**0.001**		0.092	
Danian/Selandian	-		-						0.178		**0.033**	
Thanetian	-		-		-		-					
Axes Specific	PC1		PC2		PC1		PC2		PC1		PC2	
	L	C	L	C	L	C	L	C	L	C	L	C
Maastrichtian					-	-	-	-	-	-	-	-
Danian/Selandian	**0.001**	0.429	**0.003**	0.169					-	-	-	-
Thanetian	**0.001**	0.429	0.093	**0.039**	0.692	0.189	0.055	0.169				

Table S3. False Discovery Rate adjusted *p*-values derived from the np-MANOVA pairwise comparisons between time bins in the global three-stage binning scheme. Related to Figure 2A and Table S2. L = Lamniformes; C = Carcharhiniformes.

	Maastrichtian				Danian				Selandian				Thanetian			
All Axes	L		C		L		C		L		C		L		C	
Maastrichtian	-		-		**0.001**		0.238		**0.002**		0.746		**0.001**		0.2380	
Danian	-		-		-		-		**0.001**		0.845		0.251		0.238	
Selandian	-		-		-		-		-		-		**0.001**		0.708	
Thanetian	-		-		-		-		-		-		-		-	
Axes Specific	PC1		PC2		PC1		PC2		PC1		PC2		PC1		PC2	
	L	C	L	C	L	C	L	C	L	C	L	C	L	C	L	C
Maastrichtian	-	-	-	-	-	-	-	-	-	-	-	-	-	-	-	-
Danian	**0.001**	0.566	0.322	0.402	-	-	-	-	-	-	-	-	-	-	-	-
Selandian	0.45	0.56	**0.002**	0.860	**0.001**	0.611	**0.002**	0.717	-	-	-	-	-	-	-	-
Thanetian	**0.001**	0.56	0.148	0.078	0.279	0.45	0.962	0.402	**0.001**	0.56	**0.002**	0.564	-	-	-	-

Table S4. False Discovery Rate adjusted *p*-values derived from the np-MANOVA pairwise comparisons between time bins in the global four-stage binning scheme. Related to Figure 2A, Figure S1 and Table S2. L = Lamniformes; C = Carcharhiniformes. Bold type indicates statistical significance ($P<0.05$).

	late Maastrichtian			
All Axes	L		C	
early Danian	0.145		0.349	
Axes Specific	PC1		PC2	
late Maastrichtian	L	C	L	C
early Danian	0.11	0.301	0.365	0.307

Table S5. Results (FDR adjusted p-values) of the regional-level (two-stage binning scheme) pairwise comparisons between time bins. Related to Figure 2A, Figure S2 and Table S2. L = Lamniformes; C = Carcharhiniformes.